Mixing power and hydrodynamics for different clearances of the flat blade turbine impeller

Jacek Stelmach* (ID)

Lodz University of Technology, Faculty of Process and Environmental Engineering, Wolczanska 213, 93-005 Lodz, Poland

* Corresponding author:
e-mail:
jacek.stelmach@p.lodz.pl

Abstract
In the paper, the mixing power and distributions of velocity and velocity pulsations in a baffled stirred tank with a flat blade turbine impeller placed at different distances from the bottom were determined. It was found that the mixing power reached minimum values when the relative clearance of the impeller was $C/D = 0.6 \div 0.7$. The investigations of velocity distributions using the PIV method showed the axial flow of the liquid through the impeller. This results in deviations from the typical radial-circumferential flow and changes in mixing power vs. impeller clearance versus a Rushton impeller. With a clearance corresponding to the minimum power, the flow is axial-circumferential with one circulation loop. For a flat blade turbine impeller, good mixing conditions were obtained for a clearance of $0.8 < C/D < 0.9$.

Keywords
flat blade turbine impeller (FBT), mixing power, velocity distributions, velocity pulsation distributions

1. INTRODUCTION

The flat blade turbine impeller (FBT), similarly to the turbine-disk impeller (Rushton impeller – RT), is included in the group of impellers generating radial-circumferential movement of the liquid in the stirred vessel. Literature information (Skalski, 2021; Stręk, 1975) indicates that, unlike the Rushton turbine, the mixing power of this type of impeller is significantly influenced by its distance from the bottom of the tank. At the impeller located in a relative height $H_m/D \approx 0.7$, the mixing power number reaches the lowest value. With rising electricity prices, this is an interesting observation. However, this issue has not been thoroughly investigated so far. It has been partly discussed in the suspension mixing studies (Armenante and Nagamine, 1998; Devarajulu and Loganathan, 2016; Gray, 1987). However, the authors of these works focused on determining the value of the Zwietering criterion. The dependences of the mixing power on the clearance obtained by Armenante and Nagamine (1998) and Devarajulu and Loganathan (2016) differ from each other. In addition, they show differences with the relationships of other authors (Skalski, 2021; Stręk, 1975).

However, the mixing efficiency is also influenced by the hydrodynamics in the tank. If the reduction of the mixing power is accompanied by an extension of the mixing time, the energy expenditure does not have to be reduced (Stelmach et al., 2022). Our own research (Rieger et al., 2021; Stelmach et al., 2020) shows that changes in the height of the liquid above the impeller are also accompanied by changes in the mixing power. For example, at a low liquid height above a pitched-blade turbine (PBT) impeller, there is a fairly abrupt change from axial to radial flow in the area of the impeller (Rieger et al., 2021). Similar changes may occur in the case of different distances of the impeller from the bottom, because then the height of the liquid above the impeller also changes. Knowing the velocity distributions in the tank allows you to calculate the pumping capacity of the impeller. In turn, the value of the ratio of the power number Eu to the pumping number $K_p = \dot{V}_p/(N \cdot D^3)$ can be a measure of the impeller efficiency (Stręk, 1981). A more efficient impeller should be considered one which, with the same power P, achieves a higher pumping efficiency $\dot{V}_p$.

The energy supplied by the impeller is dissipated in the liquid by a cascade of eddies. The parameter determining the course of this process is the energy dissipation rate ε (Baldi and Yianneskis, 2003; Baldi et al., 2002; de Jong et al., 2009; Delafosse et al., 2011; Kilander and Rasmuson, 2005; Saarenrinne and Piirto, 2000; Sharp et al., 1998; Sheng et al., 2000; Stelmach et al., 2019; Tanaka and Eaton, 2007)

$$\varepsilon = \nu \cdot \overline{\frac{\partial u'_j}{\partial x_i}\left(\frac{\partial u'_i}{\partial x_j} + \frac{\partial u'_j}{\partial x_i}\right)} = \frac{1}{2} \cdot \nu \cdot \overline{\left(\frac{\partial u'_i}{\partial x_j} + \frac{\partial u'_j}{\partial x_i}\right)^2} \quad (1)$$

where: ε – energy dissipation rate, m²/s³, ν – kinematic viscosity, m²/s, u'_i – i-th component of fluctuating velocity, m/s.

The practical usefulness of the definition equation for calculating the energy dissipation rate distribution in the stirred vessel is small. Therefore, it is calculated based on other relationships (Stelmach et al., 2005). The simplest of them is

$$\varepsilon = c \cdot \frac{\overline{u'}^3}{L} \quad (2)$$

www.czasopisma.pan.pl   PAN   www.journals.pan.pl
POLSKA AKADEMIA NAUK

J. Stelmach   Chem. Process Eng., 2023, 44(2), e7

where: c – coefficient, L – integral scale of eddies, m, u' – mean square velocity pulsation, m/s. The size of the largest eddies is often taken to be the diameter of the impeller D (Šulc and Ditl, 2017), but the literature also suggests the value $L = D/10$ (Zhou and Kresta, 1996a). Equation (2) is true in the case of isotropic turbulence. However, its use requires knowing the value of the coefficient c, which is determined experimentally for a given type of impeller. Unfortunately, the literature on energy dissipation in the stirred vessel focuses on the Rushton turbine. Therefore, in the case of determining maps of the ε distribution, it is convenient to use the following equation

$$\varepsilon \sim \overline{u'}^3 \qquad (3)$$

resulting from Equation (2). The information obtained on the basis of dependence (3) is only qualitative in nature, but it allows to identify areas with the greatest turbulence.

The aim of this work was to determine the mixing power and distribution of velocity and its pulsation for a flat blade turbine impeller (FBT) depending on its distance from the bottom of the tank.

2. MATERIALS AND METHODS

Tests were carried out in a flat-bottomed glass tank with internal diameter of $T = 292$ mm. A tank with four standard baffles ($B = 0.1 \cdot T$) was filled with water to a height of $H_0 = 300$ mm ($H_0 \approx T$). The six-blade FBT impeller had a diameter of $D = 100$ mm ($T/D \approx 3$) and a blade height of $b = 0.2 \cdot D = 20$ mm. The clearance of the impeller (distance of the lower edge of the impeller from the bottom) was: $C = 30, 50, 55, 60, 65, 70, 75, 80, 85, 90, 100, 110, 130$ and 150 mm. The diagram of the experimental rig is shown in Fig. 1.
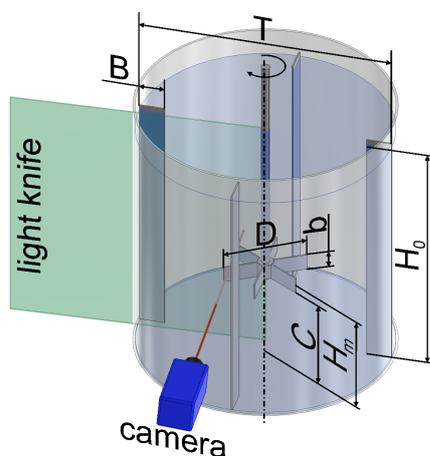
Figure 1. Scheme of the experimental rig.

To determine the mixing power, the IKA EURO-ST P CV meter was used, connected to a computer recording the instantaneous values of the impeller rotational frequency N

and torque M with the sampling time $\Delta\tau = 2$ s. The rotational frequency was smoothly changed in the range from $N = 50$ min^{-1} to $N = 400$ min^{-1}. The mixing power number Eu was then calculated from the relationship

$$\text{Eu} = \frac{P}{N^3 \cdot D^5 \cdot \rho} = \frac{2 \cdot \pi \cdot N \cdot M}{N^3 \cdot D^5 \cdot \rho} = \frac{2 \cdot \pi \cdot M}{N^2 \cdot D^5 \cdot \rho} \qquad (4)$$

The PIV system (Raffel et al., 2007; Stelmach et al., 2021) by LaVision with a two-pulse Nd:YAG laser with a maximum power of 135 mW and an ImagePro camera with a resolution of 2048×2048 px was used for velocity measurements. Glass hollow spheres with an average diameter of 10 μm added to the water served as tracers. Since the flow pattern for the dimensionless velocity does not depend on the rotational frequency of the impeller (Heim and Stelmach, 2011), the tests were carried out for one rotational frequency, which was $N = 360$ min^{-1} (Re ≈ 60000). The vertical plane of the light knife was about $2°$ in front of the baffle. The optical axis of the camera was perpendicular to the plane of the light knife. The use of the Vario-Pancolar 35–70 mm f/2.7–f/3.5 lens made it possible to obtain a measurement area of approx. 300×300 mm at the shortest focal length. For each impeller clearance, a series of 200 double photos of the flow markers in the tank were recorded with a frequency of 2.7 Hz (Heim and Stelmach, 2011) with a time interval of $\Delta\tau = 800$ µs between pulses. After two-pass image processing in the DaVis 7.2 program, distributions of instantaneous velocities were obtained in measurement fields of 32×32 px. On their basis, the program calculated average velocities and average velocity pulsations (in terms of RMS) for the radial and axial components.

3. RESULTS

3.1. Mixing power

Figure 2 shows the dependence of the mixing power number Eu on the relative clearance of the impeller C/D.

The obtained curve of power changes is consistent with the literature data (Skalski, 2021; Stręk, 1975). For $C/D \approx 1$, the number of mixing powers has the value Eu = 4.4. This is a value close to that given in the literature (Nagata, 1975; Stręk, 1981) for this impeller. Reducing the clearance decreases the mixing power. In the range from $C/D = 0.6$ to $C/D = 0.7$ the mixing power reaches the lowest value. Thus, from an energy point of view, this is the best distance between the impeller and the bottom of the tank. However, as mentioned in the introduction, the mixing efficiency is also influenced by the hydrodynamics of the liquid in the tank. Its changes include influence on mixing (homogenization) time. Therefore, before drawing final conclusions, the method of liquid circulation in the stirred vessel should be considered.

www.czasopisma.pan.pl   PAN   www.journals.pan.pl
POLSKA AKADEMIA NAUK

Chem. Process Eng., 2023, 44(2), e7   *Mixing power and hydrodynamics for different clearances of the flat blade turbine impeller*
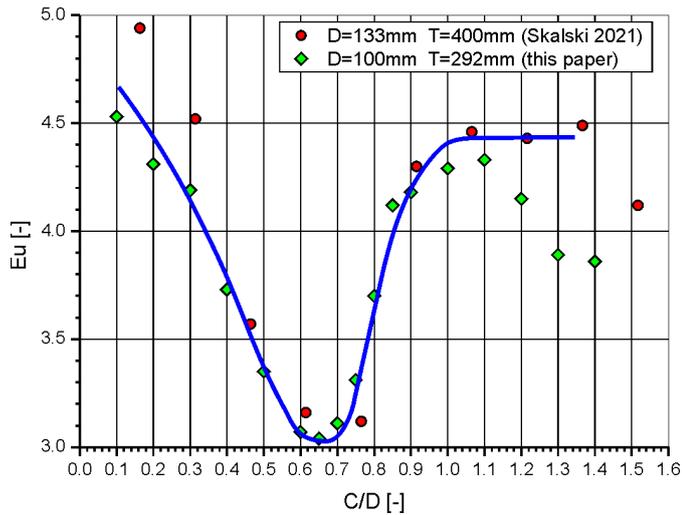
Figure 2. The dependence of the mixing power on the clearance.

3.2. Flow pattern

On the basis of the values and directions of the velocity components, the resultant velocity vectors U were determined. Figure 3 shows the distributions of dimensionless average fluid velocities in the tank $U^* = U/U_{tip} = U/(\pi \cdot D \cdot N)$ when the impeller clearance was $C/D = 1.4$ ($H_m = 150$ mm) and $C/D = 1.2$ ($H_m = 130$ mm). Dimensionless coordinates

were used to facilitate comparisons with other authors' data: $H^* = H/H_0$, $R^* = R/(D/2)$.

In both cases, there are two circulation loops in the tank, as for impellers with a classic radial flow. It is worth noting, however, that the axial liquid flow through the impeller is directed towards the top of the tank. For this reason, radial flow occurs above the impeller. Reducing the clearance moves the circulation nuclei towards the bottom, which increases the upper circulation loop. Further reduction of the clearance changes the direction of liquid flow through the mixer (Fig. 4).

For $C/D = 1.0$ ($H_m = 110$ mm) the liquid flows from above into the impeller and only below it flows radially towards the wall. As the clearance decreases, the lower circulation loop decreases. Reducing the lower circulation loop makes the flow similar to axial flow (Fig. 5).

For $C/D = 0.8$ ($H_m = 90$ mm), the lower circulation loop almost disappears, and for $C/D = 0.75$, the flow is axial and at the same time a "dead zone" of mixing is created above the bottom. When the clearance is further reduced, the stream of liquid flowing out of the mixer reaches the bottom (Fig. 6) and is slowed down by it. The "dead zone" in which the liquid has a very low velocity also disappears.

In general, the lower the impeller is placed, the stronger the effect of the bottom on the liquid stream. On the other hand,
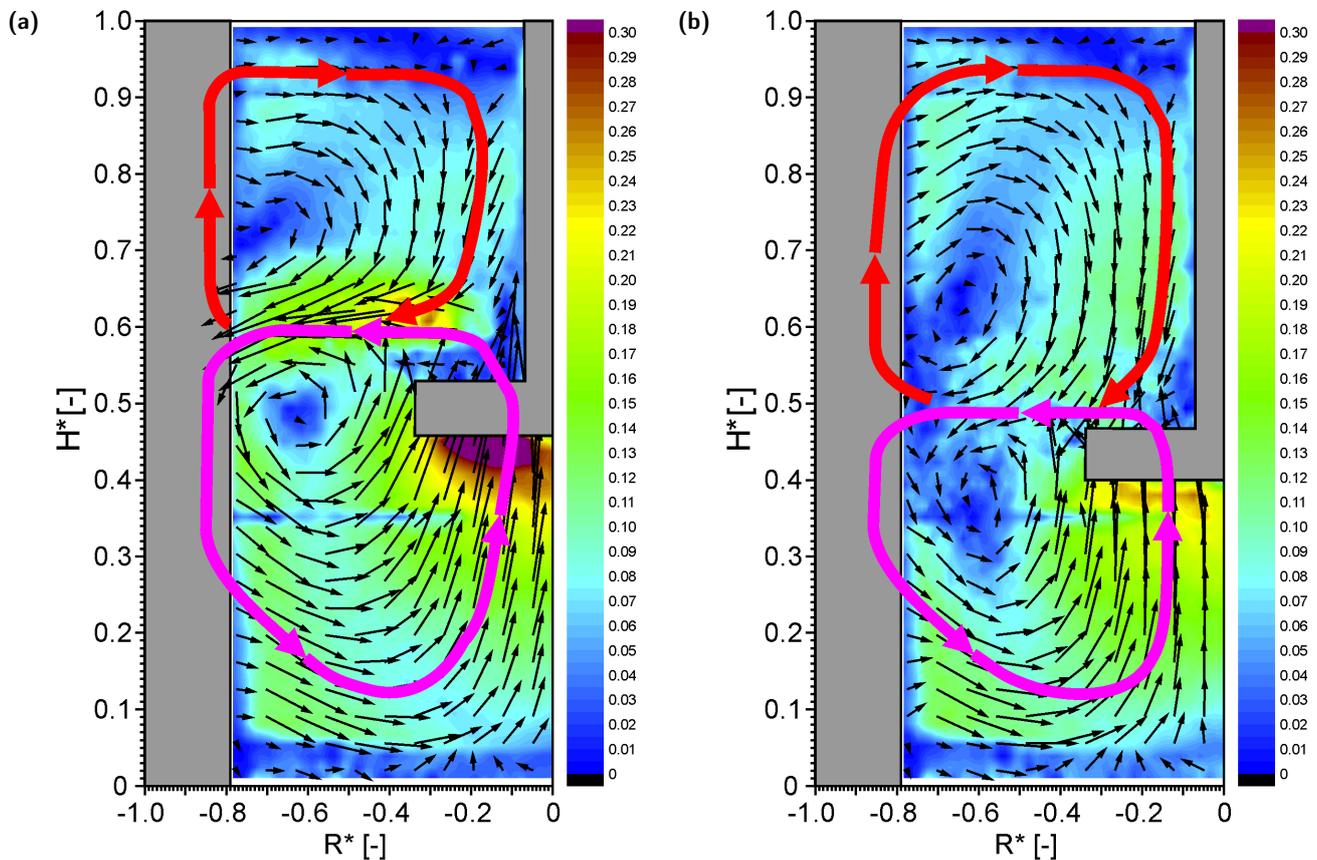
Figure 3. Liquid circulation in the stirred vessel for the upper position of the impeller: (a) $C/D = 1.4$, (b) $C/D = 1.2$.
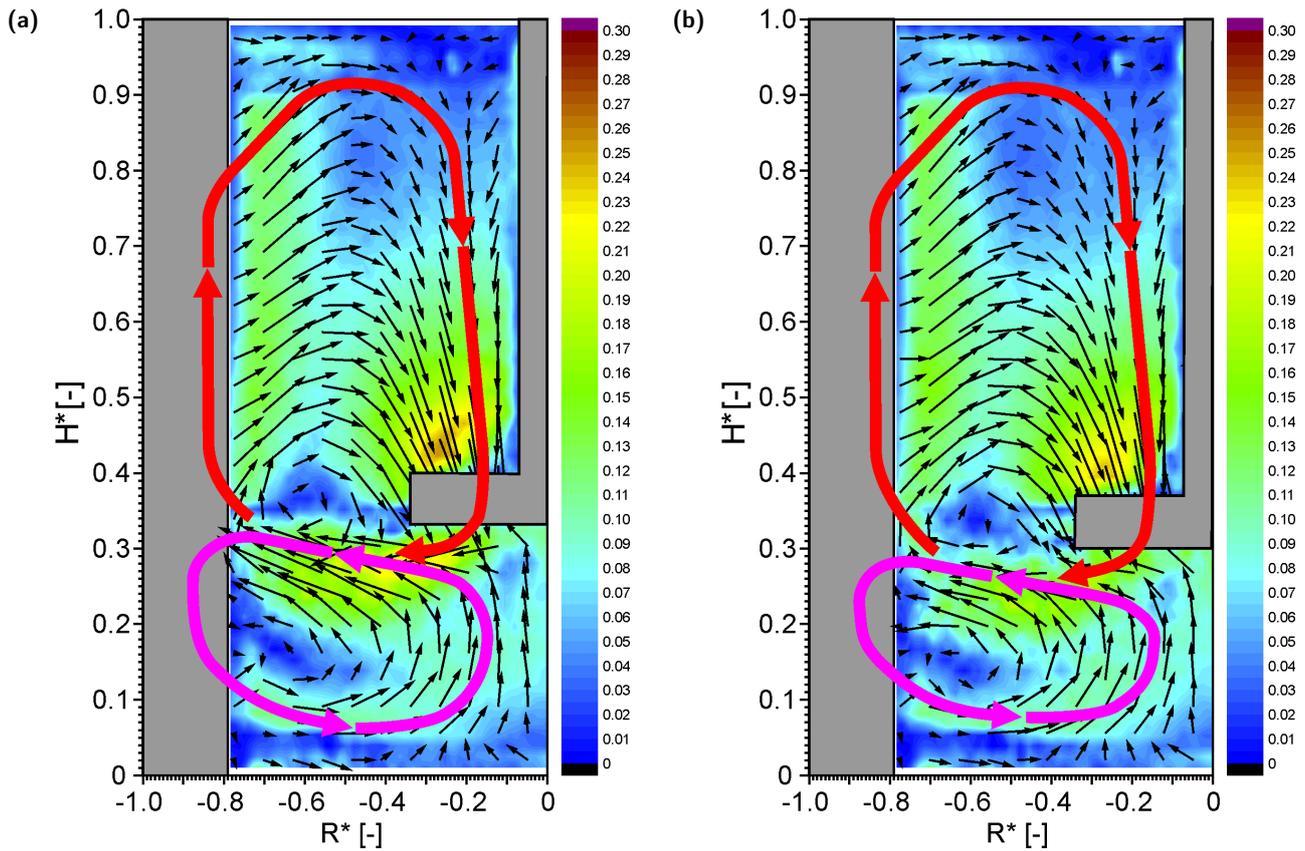
Figure 4. Liquid circulation in the stirred vessel for the middle position of the impeller: (a) $C/D = 1.0$, (b) $C/D = 0.9$.
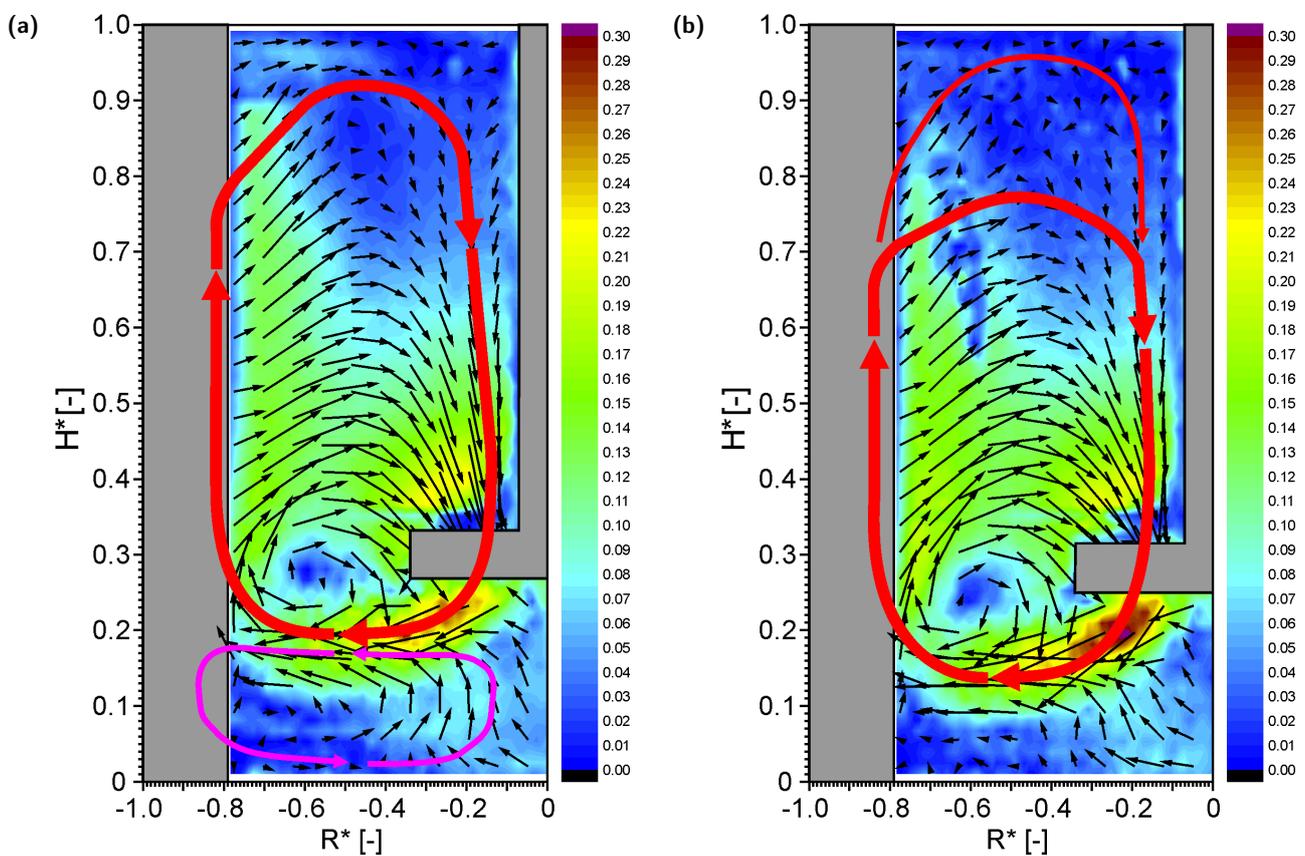
Figure 5. Liquid circulation in the stirred vessel for the lower position of the impeller: (a) $C/D = 0.8$, (b) $C/D = 0.75$.
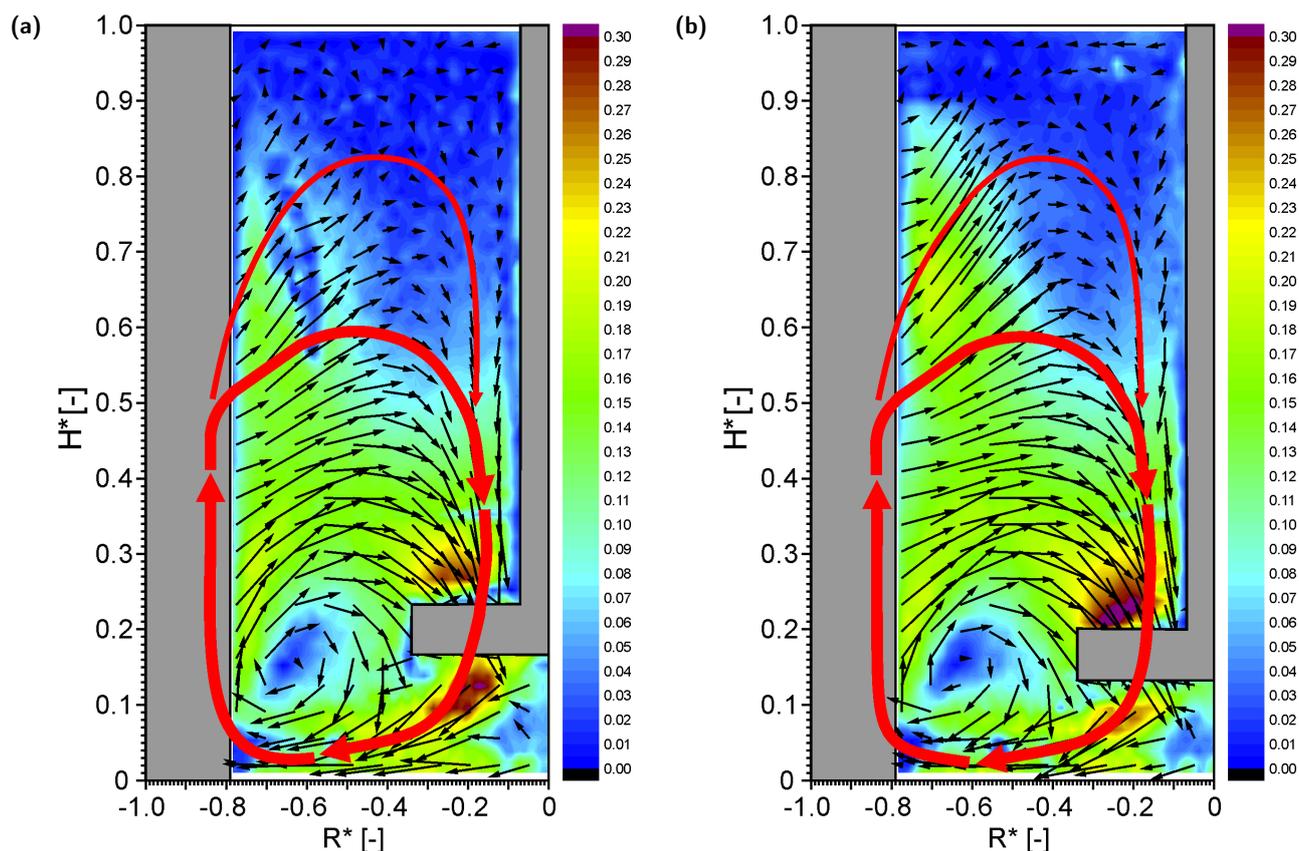
Figure 6. Liquid circulation in the stirred vessel for the lower position of the impeller: (a) $C/D = 0.5$, (b) $C/D = 0.4$.

in the upper part of the stirred vessel, practically no changes are observed.

3.3. Mixing power vs. flow pattern

Comparative analysis of the mixing power and flow pattern drawings leads to the conclusion that there is a relationship between the mixing power and the way the liquid flows (circulates) generated by the impeller. Radial flow with two liquid circulation loops is more energy-intensive (Nagata, 1975; Stręk, 1981). In contrast, in the case of the FBT impeller, reducing the clearance leads to a flow similar to the less energy-intensive axial flow. However, typical axial flow impellers have much lower mixing powers. For example, for a six-blade pitched blade turbine impeller (PBT) with a blade inclination of $45°$ and $C/D = 0.9$, the power number is Eu = 1.58 (Nagata, 1975; Stręk, 1981). Therefore, the operation of FBT impellers with too small a clearance is not effective – better results will be obtained by using typical impellers generating axial flow. The minimum value of the power number is reached when the stream of liquid flows towards the bottom, but is not strongly decelerated by it. The influence of the bottom must be large, because for clearances $C/D < 0.3$, the mixing power increases to the value as for $C/D = 1$.

3.4. Pumping capacity

For radial impellers, the pumping capacity understood as the volumetric flow rate of liquid outflow from the impeller area in the radial direction for $R = D/2$ is

$$\dot{V}_p = \pi \cdot D \cdot \int_{-b/2}^{b/2} U_r(H) \cdot dH \qquad (5)$$

Figure 7a shows radial velocity profiles at a distance of $R = 51$ mm ($R^* = 0.35$) from the tank axis. The dimensionless heights of the impeller suspension H_m^* calculated from the relationship

$$H_m^* = \frac{H - H_m}{H_0} \qquad (6)$$

were placed on the ordinate axis, which significantly facilitated the analysis of profiles in relation to the position of the impeller (the middle of the height of the impeller corresponds to the value $H_m^* = 0$).

For high positions of the impeller, the maximum radial velocities occur above the impeller (Fig. 7a). When the clearance C/D is smaller than 1.10, the radial velocity maxima occur under the impeller at a distance of $\Delta H_m^* \approx 0.12$. For the clearance $C/D = 0.85$ under the lower edge of the impeller, the dimensionless velocity $U_r^* \approx 0$, which can be considered as the moment of creating one circulation loop.
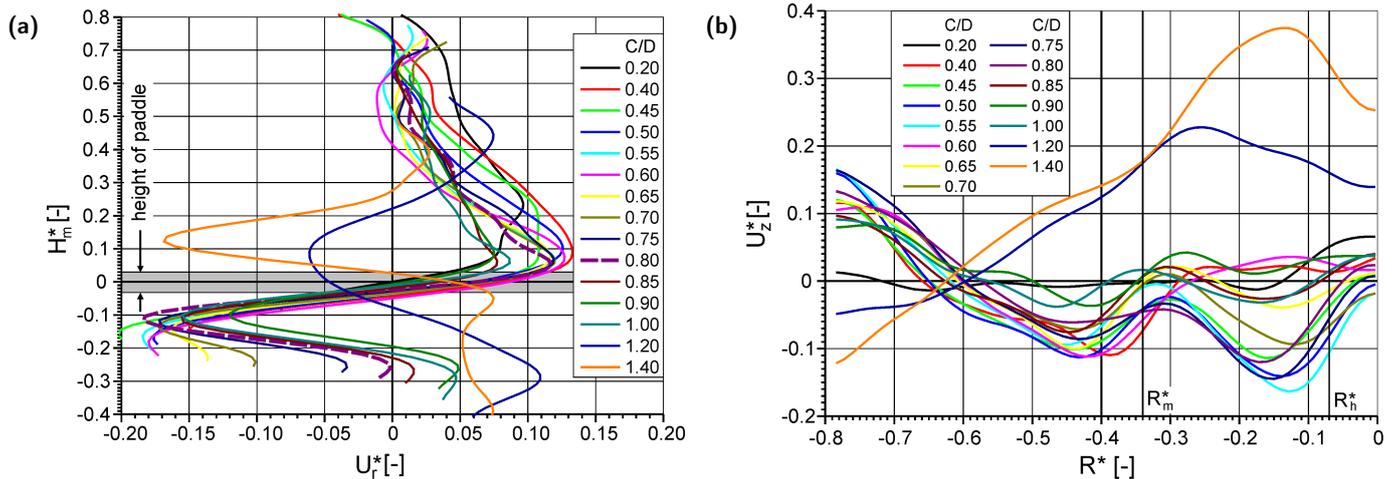
Figure 7. Velocity profiles: (a) radial component, (b) axial component.

Since the velocity maxima are not at the height of the impeller, the values calculated from Equation (5) will not correspond to the real liquid stream flowing radially towards the wall. Although this flux can be determined based on the radial velocity profile (Fig. 7a), it is not known what integration limits should be assumed. As a result, the pumping capacity cannot be calculated from the definition formula (5). However, Fig. 7a shows that for clearances $0.5 < C/D < 1.0$, the velocity profiles under the impeller are similar, and therefore the radial flowing liquid streams will also be similar.

Since the FBT impeller also generates axial flow, Fig. 7b shows the axial velocity profiles under the impeller. The highest values of the axial component are achieved for clearances $0.65 < C/D < 0.75$, which also corresponds to the minimum mixing power. Outside this range, the axial velocity profiles flatten out, which means a reduction in axial flux. It is worth noting that the changes in the shape of the axial velocity profiles in Fig. 7b correspond to the course of the mixing power curve in Fig. 2.

3.5. Velocity pulsations

Figures 8, 9 and 10 show maps (contour plots) of dimensionless pulsations of radial and axial velocities ($\overline{u'}^* = \overline{u'}/U_{tip}$). The purple line is the area where the pulsations exceed 20% of the paddle tip velocity U_{tip} and the red line is the area where the pulsations are above 25% of the U_{tip} velocity.

For high positions of the impeller, when the liquid flow through the impeller is directed upwards (Fig. 8a), the largest velocity pulsations occur above the impeller in the area of $0.25 < R^* < 0.45$ and $0.53 < H^* < 0.63$. Changing the direction of the liquid flow through the impeller moves the area of the largest pulsations under the impeller and significantly increases it (Fig. 8b), especially in the radial direction ($0.20 < R^* < 0.65$ and $0.23 < H^* < 0.33$). Thus, the largest pulsations were always in the stream flowing out of the impeller area, which is consistent with the phenomenal flow analysis. Further lowering of the impeller intensifies the velocity pulsations (Fig. 9).
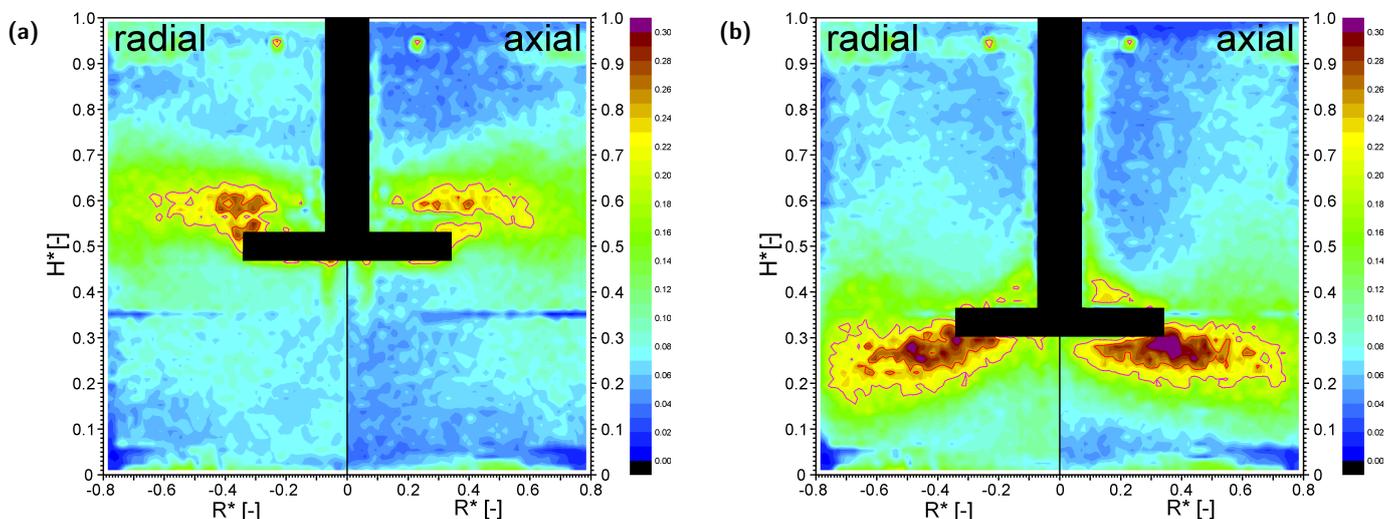
Figure 8. Velocity pulsation distributions for the upper position of the impeller: (a) $C/D = 1.4$, (b) $C/D = 0.9$.
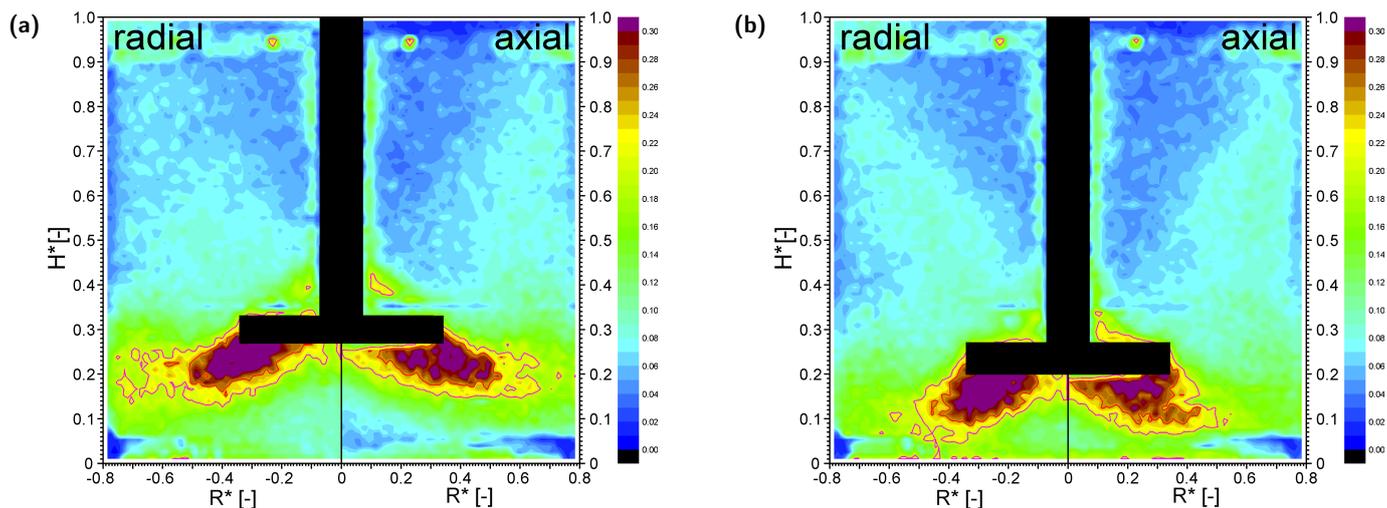
Figure 9. Velocity pulsation distributions for the middle position of the impeller: (a) $C/D = 0.8$, (b) $C/D = 0.6$.
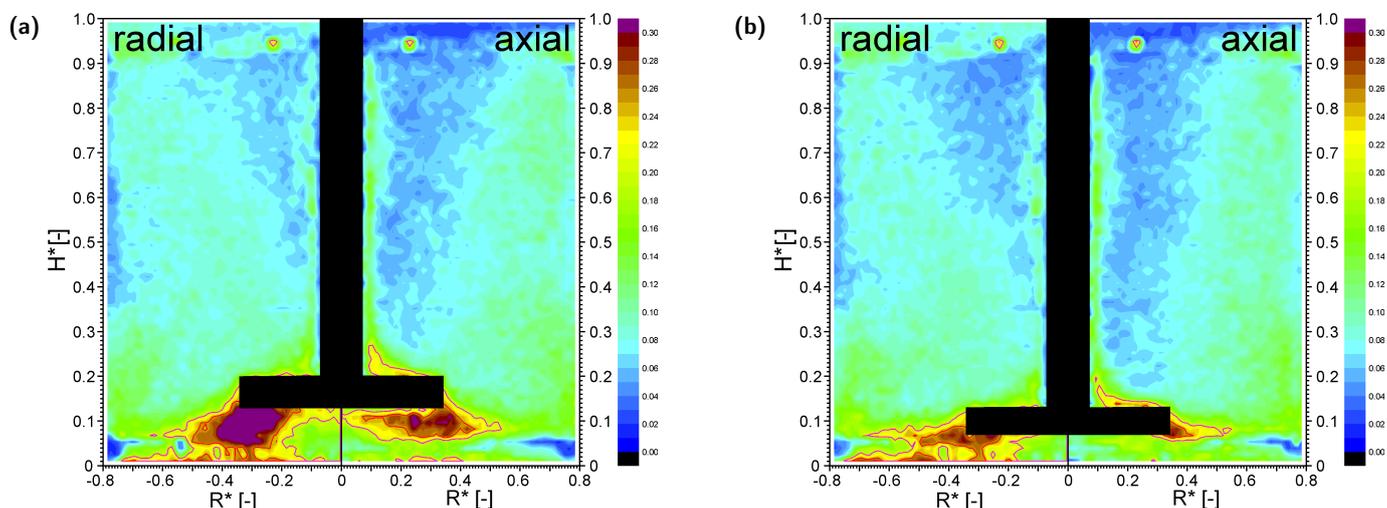
Figure 10. Velocity pulsation distributions for the lower position of the impeller: (a) $C/D = 0.4$, (b) $C/D = 0.2$.

For $C/D = 0.8$ (Fig. 9a) the area of pulsations exceeding 25% U_{tip} increases, while the area $\overline{u'}^* > 25\% U_{\text{tip}}$ practically does not change compared to the clearance $C/D = 0.9$. With the clearance $C/D = 0.6$, the area $\overline{u'}^* > 25\% U_{\text{tip}}$ does not change its size, but the area $\overline{u'}^* > 20\% U_{\text{tip}}$ decreases (Fig. 9b). Further reduction of the clearance significantly influences the velocity pulsation distributions (Fig. 10).

For the clearance $C/D = 0.4$, in the area under the impeller, the difference between radial and axial pulsations is visible (Fig. 10a). Most likely, this is due to the influence of the bottom on the movement of the liquid. The proximity of the bottom inhibits the axial movement of the liquid, and thus also the velocity pulsations. However, at this clearance, the radial motion is not strongly inhibited and the similarity of the speed pulsation distribution to larger clearances is visible. For the smallest tested clearance $C/D = 0.2$, the inhibitory effect of the bottom on the movement of the liquid is visible for both components of the velocity pulsation (Fig. 10b). The graphs shown in Figs. 8÷10 correlate well with the analyzed

method of liquid flow in the mixer shown in Figs. 4÷6. In the absence of axial flow (e.g. self-aspirating disk impeller), the maximum values of velocity pulsation occur at the height of the impeller (Micheletti et al., 2004; Stelmach et al., 2019). The analysis of Figs. 8÷10 shows that most of the energy is dissipated near the impeller, which is consistent with the information in the literature (Ng and Yianneskis, 2000; Zhou and Kresta, 1996b).

By summing the local velocity pulsations to the power of 3, the value of the coefficient c in Equation (2) can be determined, since this sum should be equal to the mixing power. However, this requires taking measurements in different planes between the partitions. For the tested plane approx. $2°$ in front of the baffle, the results are shown in Fig. 11a.

For the tested plane, the course of the points differs from the course of the mixing power curve, but it is not representative for the entire stirred vessel. In the range of $0.4 < C/D < 1.2$,
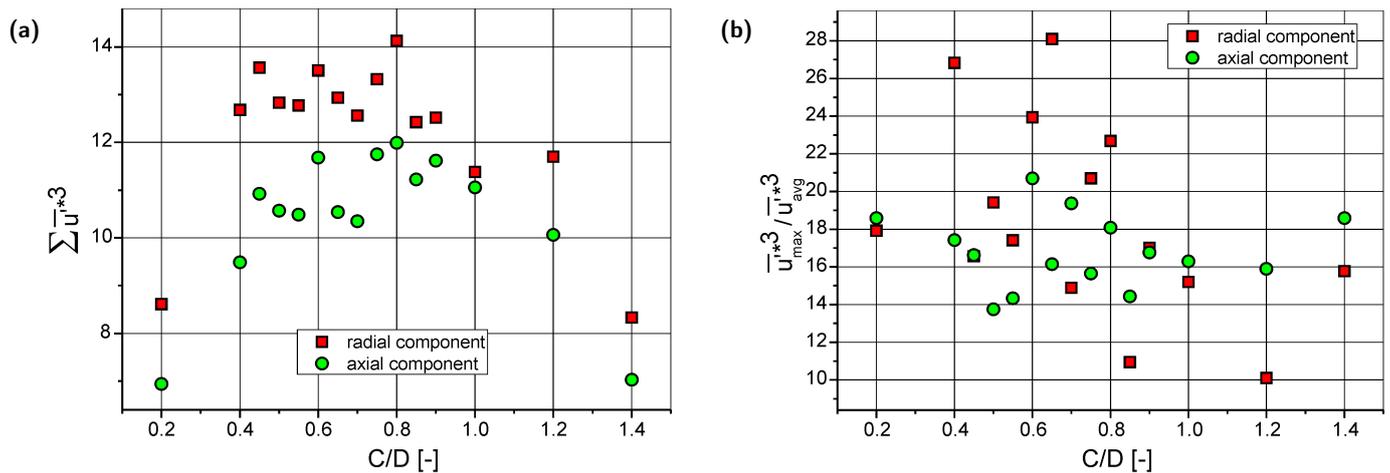
Figure 11. Velocity pulsations in the power of 3 in the measurement plane: (a) sum, (b) maximum value related to the average value.

it is possible to assume the value of the velocity pulsation sums to be constant. On the other hand, Fig. 11b shows the dependence of the maximum pulsation value related to the average value. This value ranges from 10 to 28. Similar values can be found in the literature for the Rushton turbine (Kresta, 1998; Sharp et al., 1998), although other sources give higher values (Šulc and Ditl, 2017; Zhou and Kresta, 1996b).

The size of the area in which the mean square velocity pulsations exceed $20\% \cdot U_{tip}$ is on average 8.4% for the radial component and 6.8% for the axial component in relation to the entire cross-section of the tank. This suggests that the turbulence is not isotropic near the impeller.

4. CONCLUSIONS

Unlike the Rushton impeller, the design of the FBT impeller allows liquid to flow axially between the blades. This has a significant impact on the distribution of liquid velocity in the stirred vessel depending on the impeller clearance, i.e. the height of its suspension. A typical radial-circumferential flow can only be considered for a clearance of $C/D = 1.1$ (at $H_0 = T$). For clearances $C/D > 0.75$, there are two liquid circulation loops, and for $C/D < 0.75$, there is only one circulation loop in the vessel, as for axial flow impellers (PBT, propeller).

Changes in hydrodynamics are accompanied by changes in mixing power. Starting from $C/D < 1.0$, reducing the clearance decreases the mixing power number Eu. The mixing power reaches a minimum value in the range of $C/D = 0.6$ to $C/D = 0.7$. In this range of clearances, the FBT impeller generates axial flow, but the power number is about twice as high as for a classic radial impeller, i.e. a PBT impeller with a 45° angle of inclination of the blades.

Due to the method of liquid circulation in the stirred vessel with the FBT impeller, the calculation of the pumping efficiency of the impeller from the definition formula (Equation (5)) will be burdened with a large error for most clearances. The axial liquid flow through the impeller causes the radial liquid flow at the height of the impeller to be small. Radial velocity maxima are observed above or below the impeller. Only with a clearance of $C/D = 1.1$ ($H_m = 120$ mm) the liquid flows radially from the impeller.

In the range of clearances from $C/D = 1.4$ to $C/D = 0.5$, outside the area near the impeller, the distributions of radial and axial velocities pulsations are similar. Therefore, for these components, for the area outside the impeller (bulk zone), the turbulence can be defined as isotropic.

The analysis of the test results shows that the distance H_m of the FBT mixer from the bottom should be slightly smaller than its diameter D, so that the clearance meets the condition $0.8 < C/D < 0.9$.

SYMBOLS

B	baffle width, m
b	paddle height, m
C	clearance, m
c	coefficient,
D	impeller diameter, m
H	height (generally), m
H_0	liquid height in the tank, m
H_m	distance of the impeller height center from the bottom, m
H_m^*	dimensionless heights of the impeller suspension,
H^*	dimensionless height, $H^* = H/H_0$
L	integral scale of eddies, m
M	torque, Nm
N	rotational frequency of the impeller, s^{-1}
P	power, W

www.czasopisma.pan.pl   PAN   www.journals.pan.pl
POLSKA AKADEMIA NAUK

Chem. Process Eng., 2023, 44(2), e7   *Mixing power and hydrodynamics for different clearances of the flat blade turbine impeller*

R radius (generally), m

R^* dimensionless radius, $R^* = R/(D/2)$

T tank diameter, m

U velocity, m/s

U_{tip} tangential velocity of the blade tip, $U_{tip} = \pi \cdot D \cdot N$, m/s

U^* dimensionless velocity $U^* = U/U_{tip}$,

u' velocity pulsation (fluctuation), m/s

$\overline{u'}$ velocity pulsation in RMS sense, m/s

$\dot{V}_p$ pumping capacity, m³/s

Greek letters

ε energy dissipation rate, m²/s³

ρ density, kg/m³

ν kinematic viscosity, m²/s

$\Delta\tau$ time interval, s

Dimensionless numbers

Eu   Euler (power) number, $Eu = \dfrac{P}{N^3 \cdot D^5 \cdot \rho}$

K_P pumping number, $K_P = \dfrac{\dot{V}_p}{N \cdot D^3}$

Re   Reynolds number for mixing process, $Re = \dfrac{N \cdot D^2}{\nu}$

REFERENCES

Armenante P.M., Nagamine E.U., 1998. Effect of low off-bottom impeller clearance on the minimum agitation speed for complete suspension of solids in stirred tanks. *Chem. Eng. Sci.*, 53, 1757–1775. DOI: 10.1016/S0009-2509(98)00001-3.

Baldi S., Hann D., Yianneskis M., 2002. On the measurements of turbulence energy dissipation in stirred vessels with PIV techniques. *Proceedings of the 10th International Symposium on Applications of Laser Techniques to Fluid Mechanics*, Lisbon, Portugal.

Baldi S., Yianneskis M., 2003. On the direct measurement of turbulence energy dissipation in stirred vessels with PIV. *Ind. Eng. Chem. Res.*, 42, 7006–7016. DOI: 10.1021/ie0208265.

de Jong J., Cao L., Woodward S.H., Salazar J.P.L.C., Collins L.R., Meng H., 2009. Dissipation rate estimation from PIV in zero-mean isotropic turbulence. *Experiments in Fluid*, 46, 499–515. DOI: 10.1007/s00348-008-0576-3.

Delafosse A., Collignon M.-L., Crine M., Toye D., 2011. Estimation of the turbulent kinetic energy dissipation rate from 2D-PIV measurements in a vessel stirred by an axial Mixel TTP impeller. *Chem. Eng. Sci.*, 66, 1728–1737. DOI: 10.1016/j.ces.2011.01.011.

Devarajulu C., Loganathan M., 2016. Effect of impeller clearance and liquid level on critical impeller speed in an agitated vessel using different axial and radial impellers. *J. Appl. Fluid Mech.*, 9, 2753-2761. DOI: 10.29252/jafm.09.06.24824.

Gray D.J., 1987. Impeller clearance effect on off bottom particle suspension in agitated vessels. *Chem. Eng. Commun.*, 61, 151–158. DOI: 10.1080/00986448708912035.

Heim A., Stelmach J., 2011. The comparison of velocities at the self-aspirating disk impeller level. *Przemysł Chemiczny*, 90/9, 1642–1646.

Kilander J., Rasmuson A., 2005. Energy dissipation and macro instabilities in a stirred square tank investigated using an LE PIV approach and LDA measurements. *Chem. Eng. Sci.*, 60, 6844–6856. DOI: 10.1016/j.ces.2005.02.076.

Kresta S., 1998. Turbulence in stirred tanks: Anisotropic, approximate, and applied. *Can. J. Chem. Eng.*, 76, 563–576. DOI: 10.1002/cjce.5450760329.

Micheletti M., Baldi S., Yeoh S.L., Ducci A., Papadakis G., Lee K.C., Yianneskis M., 2004. On spatial and temporal variations and estimates of energy dissipation in stirred reactors. *Chem. Eng. Res. Des.*, 82, 1188–1198. DOI: 10.1205/cerd.82.9.1188.44172.

Nagata S., 1975. *Mixing. Principles and applications*. John Wiley & Sons, New York, NY, USA.

Ng K., Yianneskis M., 2000. Observations on the distribution of energy dissipation in stirred vessels. *Chem. Eng. Res. Des.*, 78, 334–341. DOI: 10.1205/026387600527446.

Raffel M., Willert C., Wereley S., Kompenhans J., 2007. *Particle image velocimetry. A practical guide*. 2nd edition, Springer Berlin, Heidelberg.

Rieger F., Moravec J., Stelmach J., Kuncewicz Cz., 2021. Effect of modification of the stirrer with folding blades on the increase in mixing power during emptying the tank. *Przemysł Chemiczny*, 100/12, 1231–1235. DOI: 10.15199/62.2021.12.15.

Saarenrinne P., Piirto M., 2000. Turbulent kinetic energy dissipation rate estimation from PIV vector fields. *Exp. Fluids*, 29 (Suppl 1), S300–S307. DOI: 10.1007/s003480070032.

Sharp K.V., Kim K.C., Adrian R., 1998. Dissipation estimation around a Rushton turbine using particle image velocimetry. *Proceedings of the 9th International Symposium on Applications of Laser Techniques to Fluid Mechanics*, Lisbon, Portugal.

Sheng J., Meng H., Fox R.O., 2000. A large eddy PIV method for turbulence dissipation rate estimation. *Chem. Eng. Sci.*, 55, 4423–4434. DOI: 10.1016/S0009-2509(00)00039-7.

Skalski M., 2021. Investigation of the dependence of the mixing power on the distance between the impeller and the bottom of the tank. Eng. Thesis, Lodz University of Technology, Lodz, Poland (in Polish).

Stelmach J., Kuncewicz Cz., Rieger F., Moravec J., Jirout T., 2020. Increase of mixing power during emptying of tanks with turbine-blade impellers. *Przemysł Chemiczny*, 99/2, 239–243. DOI: 10.15199/62.2020.2.11.

Stelmach J., Kurasiński T., Kuncewicz Cz., 2005. Comparative analysis of selected methods for calculation of energy dissipation rate. *Chem. Process Eng.*, 26, 201–215.

Stelmach J., Musoski R., Kuncewicz Cz., Głogowski M., 2019. Turbulent energy dissipation rate and turbulence scales in the blade region of a self-aspirating disk impeller. *J. Appl. Fluid Mech.*, 12, 715–728. DOI: 10.29252/jafm.12.03.28836.

Stelmach J., Musoski R., Kuncewicz Cz., Jirout T., Rieger F., 2022. Efficiency of PBT impellers with different blade cross-sections. *Energies*, 15, 585. DOI: 10.3390/en15020585.

Stelmach J., Musoski R., Mysakowski T., 2021. Analysis of the efficiency of PBT stirrers depending on the clearance. *Przemysł Chemiczny*, 100/8, 762–766. DOI: 10.15199/62.2021.8.8.

Stręk F., 1975. Mixing and stirrers. Chemistry, Leningrad.

Stręk F., 1981. *Mieszanie i mieszalniki*. WNT, Warszawa.

Šulc R., Ditl P., 2017. Local turbulent energy dissipation rate in an agitated vessel: New approach to dimensionless definition. *Theor. Found. Chem. Eng.*, 51, 159–174. DOI: 10.1134/S0040579517020105.

Tanaka T., Eaton J.K., 2007. A correction method for measuring turbulence kinetic energy dissipation rate by PIV. *Exp. Fluids*, 42, 893–902. DOI: 10.1007/s00348-007-0298-y.

Zhou G., Kresta S.M., 1996a. Distribution of energy between convective and turbulent flow for three frequently used impellers. *Chem. Eng. Res. Des.*, 74, 379–389.

Zhou G., Kresta S.M., 1996b. Impact of tank geometry on the maximum turbulence energy dissipation rate for impellers. *AIChE J.*, 42, 2476–2490. DOI: 10.1002/aic.690420908.